Quantitative Confocal Imaging of the Retinal Microvasculature in the Human Retina

Priscilla Ern Zhi Tan,[1,2] *Paula K. Yu,*[1,2] *Chandrakumar Balaratnasingam,*[1,2] *Stephen J. Cringle,*[1,2] *William H. Morgan,*[1] *Ian L. McAllister,*[1] *and Dao-Yi Yu*[1,2]

Purpose. We investigated quantitatively the distribution of blood vessels in different neural layers of the human retina.

Methods. A total of 16 human donor eyes was perfusion-fixed and labeled for endothelial f-actin. Retinal eccentricity located 3 mm superior to the optic disk was studied using confocal scanning laser microscopy. Immunohistochemical methods applied to whole-mount and transverse sections were used to colocalize capillary networks with neuronal elements. Capillary morphometry, diameter, and density measurements were compared among networks.

Results. Four different capillary networks were identified and quantified in the following regions: Nerve fiber layer (NFL), retinal ganglion cell (RGC) layer, border of the inner plexiform layer (IPL) and superficial boundary of the inner nuclear layer (INL), and boundary of the deep INL and outer plexiform layer. The innermost and outermost capillary networks demonstrated a laminar configuration, while IPL and deep INL networks displayed a complex three-dimensional configuration. Capillary diameter in RGC and IPL networks were significantly less than in other networks. Capillary density was greatest in the RGC network (26.74%), and was significantly greater than in the NFL (13.69%), IPL (11.28%), and deep INL (16.12%) networks.

Conclusions. The unique metabolic demands of neuronal subcompartments may influence the morphometric features of regional capillary networks. Differences in capillary diameter and density between networks may have important correlations with neuronal function in the human retina. These findings may be important for understanding pathogenic mechanisms in retinal vascular disease. (*Invest Ophthalmol Vis Sci.* 2012;53:5728–5736) DOI:10.1167/iovs.12-10017

The precise organization of vascular structures within the human retina allows the optical properties of the eye, and the nutritional demands of retinal structures, to be maintained simultaneously. A change in capillary network density, in response to altered retinal homeostasis, is likely to modify the refractive properties of the light path to the outer retina. Similarly, changes in capillary morphometry, as a means of improving retinal optics, may compromise nutritional supply to important neuronal elements.

Concepts regarding the role of neurons in modulating regional blood flow, and thereby the local supply of glucose and oxygen, have undergone significant paradigm shifts over the past decade.[1] Previous researchers favored the idea that local blood flow was controlled by negative feedback mechanisms; however, there now is increasing evidence to suggest that neurons and glial cells have a vital role in controlling the capillary circulation.[1,2] Understanding the morphometric organization of capillary systems in the human retina, and the relationship they bear to distinct neuronal layers, may increase our understanding of neurovascular coupling mechanisms that are important in retinal homeostasis.[2] Detailed knowledge of neuron-glial-vascular interactions in the retina also may provide insights into pathogenic mechanisms relevant to retinal vascular diseases.

Oxygen is an essential substrate for retinal energy metabolism and has a key role in moderating neurovascular coupling mechanisms.[1] Intraretinal oxygen distribution and uptake has been quantified precisely in the mammalian retina and the disparities in metabolic activity between somal, dendritic, and synaptic retinal compartments have been demonstrated previously.[3–8] Although it has been known for decades that the multilayered retinal capillary network underlies the distribution of oxygen tension in the retina[9] the relationships between capillary network morphometry and the heterogeneous metabolic demands of neuronal elements remain unclarified. Gariano et al. documented the location of vascular plexuses within the primate retina, and performed detailed quantitative measurements of the temporal and spatial sequence of vascular plexus formation.[10] These studies have been critical for understanding physiologic mechanisms that govern retinal angiogenesis and vascular development. Delineating the morphometric characteristics of capillary networks may identify important vascular adaptations that allow the unique metabolic demands of each retinal layer to be satisfied. It also may allow important correlations between capillary network morphometry and previously determined retinal oxygen measurements to be performed, thus allowing speculation concerning structure-function relationships in the primate retina. Finally, it may elucidate structural mechanisms that facilitate the fine balance between optical clarity and cellular nutrition in the human eye.

In this report we use novel, micropipette and antibody-based perfusion methodology, together with confocal microscopic techniques, to examine the retinal circulation.[11–13] The region of retina 3 mm superior to the optic disk was examined and the morphometric features of capillary networks, respective to distinct retinal layers, were quantified. A region superior to the optic disk was chosen for examination in an effort to avoid the macula – an area with vascular and cellular

From the [1]Centre for Ophthalmology and Visual Science and [2]The ARC Centre of Excellence in Vision Science, The University of Western Australia, Perth, Australia.

Supported by the National Health and Medical Research Council of Australia and the Australian Research Council Centre of Excellence in Vision Science.

Submitted for publication April 12, 2012; revised June 26, 2012; accepted July 23, 2012.

Disclosure: **P.E.Z. Tan**, None; **P.K. Yu**, None; **C. Balaratnasingam**, None; **S.J. Cringle**, None; **W.H. Morgan**, None; **I.L. McAllister**, None; **D.-Y. Yu**, None

Corresponding author: Dao-Yi Yu, Centre for Ophthalmology and Visual Science and the ARC Centre of Excellence in Vision Science, The University of Western Australia, Nedlands, Western Australia 6009; dyyu@lei.org.au.

Table 1. Human Donor Details

Donor ID	Age	Sex	Eye	Cause of Death	Time to Cannulation (h)
A	22	M	L	MVA	15.0
B	32	M	L	MVA	20.0
C	49	F	L + R	Cancer	5.5
D	67	M	L	Cancer	9.5
E	23	M	L	Suicide	22.0
F	66	M	L + R	Cancer	15.0
G	22	M	L	Suicide	15.0
H	53	M	L	MVA	14.0
I*	60	M	L	Collapse	18.0
J*	72	M	R	Drowning	15.0
K†	72	F	L	Sepsis	3.0
L‡	60	M	R	Liver disease	3.5
M	59	M	R	Melanoma	12.0
N	39	M	L	Sepsis	20.0

Age (years), sex (M, male; F, female), side (L, left; R, right) cause of death, and time to cannulation for each eye donor are provided. MVA, motor vehicle accident.

* Donor eyes that were flat-mounted for colocalization studies.

† Donor eye that was used for epoxy sectioning.

‡ Donor eye that was sectioned transversely for colocalization.

specializations that is markedly different from most other retinal eccentricities.[14] Our study is a detailed quantitative assessment of capillary networks that comprise the human retinal circulation and is an important extension to previous studies that have evaluated retinal vascular characteristics.[10,15–17]

Materials and Methods

Our study was approved by the human research ethics committee at The University of Western Australia. All human tissue was handled according to the tenets of the Declaration of Helsinki.

Human Donor Eyes

A total of 16 eyes from 14 donors was studied. All eyes were obtained from the Lions Eye Bank (Lions Eye Institute, Western Australia). Eyes were received after removal of corneal buttons for transplantation. None of the donors had a known history of eye disease. The demographic data, cause of death, and postmortem time to eye perfusion for each donor are presented in Table 1. We used 12 eyes for quantitative analysis, three eyes for colocalization studies, and one for epoxy sectioning (Table 1).

Perfusion Labeling of Retinal Circulation

Our previous reports have provided a detailed review of the perfusion-based techniques used for targeted retinal endothelial labeling.[12,13] Identical methodology was used for our present study. Briefly, the central retinal artery was cannulated, and residual blood was washed out with oxygenated Ringer's solution and 1% bovine serum albumin. After the 20-minute Ringer's wash, 4% paraformaldehyde in 0.1 M phosphate buffer was perfused for at least 30 minutes to achieve fixation. Then, 0.1% Triton-X-100 in 0.1 M phosphate-buffered solution was perfused for 5 to 7 minutes to aid in the permeation of endothelial cell membranes. Detergent subsequently was washed out by a 30-minute perfusion with 0.1 M phosphate-buffered solution. Microfilaments and cell nuclei then were labeled over the course of 2 hours by using a mixture of phalloidin conjugated to Alexa Fluor 546 (30U; Invitrogen, Carlsbad, CA) and bisbenzamide (H33258, 1.2 μg/ml; Sigma-Aldrich, St. Louis, MO) or iodide dye (YO-PRO-1, 6.6 μM; Invitrogen). Residual label was cleared from the vasculature by further perfusion with 0.1 M phosphate buffer. The posterior chamber then was immersion fixed in 4% paraformaldehyde overnight.

Tissue Preparation and Immunolabeling

The posterior globe was dissected at the equator to allow viewing of the posterior retina. The retina was dissected carefully around optic disc edge. A few cuts were made in the peripheral retina to enable the retina to lie flat.

Retinas from two separate donors (Table 1) underwent whole-mount immunolabeling using the protocol described by Xiao and Hendrickson.[18] This permitted colocalization of capillary networks relative to distinct retinal layers. In brief, the whole retina was washed in 0.1 M phosphate buffer on a shaker for one to two days, floated in 1% sodium borohydride in phosphate buffer overnight, cryoprotected in 30% sucrose and stored at −80°C. The retina subsequently was thawed and maintained at 4°C on a slow speed shaker before immunolabeling. The retina was permeabilized overnight in solution comprising 0.1% sodium azide and 0.1% Triton-X 100 in 0.1 M phosphate buffer. The solution then was changed to a blocking serum comprising 10% normal goat serum in phosphate buffer for overnight incubation. Primary antibodies then were added to the solution for incubation over three to four days. Excess antibodies were washed off by overnight incubation in 0.1 M phosphate buffer. The retina then was incubated with secondary antibodies and nucleic acid label overnight, and washed thoroughly in solution for at least 2 hours before mounting.

Retinal ganglion cells and their axons were labeled using rabbit anti-γ-synuclein[19] (1:200, Abcam ab55424; Abcam, Cambridge, MA) and goat anti-rabbit secondary antibody conjugated to Alexa Fluor 488 (1:200, Invitrogen A11034; Invitrogen). For identification of ON-bipolar cells[20] and horizontal cells,[20] the primary antibodies that were used included mouse anti-Go-α (1:100, Millipore MAB3073; Millipore, Billerica, MA) and rabbit anti-parvalbumin (1:200, Swant PV 25; Swant, Marly, Fribourg), respectively. Secondary antibodies that were conjugated to these primary antibodies included goat anti-mouse antibody (Alexa Fluor 488, 1:200, Invitrogen A10680; Invitrogen) and goat anti-rabbit antibody (Alexa Fluor 635, 1:200, Invitrogen A21070; Invitrogen), respectively. Separate retinas were used for labeling retinal ganglion cells and horizontal cells, as the secondary antibodies for both primary antibodies were derived from rabbit species.

One eye that did not undergo perfusion-labeling was used for immunolabeling colocalization after frozen sectioning (Table 1). The same retinal eccentricity was examined. Transverse retinal frozen sections, 12 μm thick, were dried onto Gold slides (Erie Superfrost PLUS, ERIFT-4981GLPLUS-006E; Biolab, Decatur, GA) and used for immunolabeling. Blood vessels were labeled using lectins from Triticum Vulgaris conjugated to TRITC (1:50, Sigma L5266; Sigma-Aldrich). Nuclei were counter-labeled using bisbenzamide (H33258, 1.2μg/ml; Sigma-Aldrich). Remaining primary and secondary antibodies that were used for colocalization studies in these transverse sections were the same as that described above for whole-mount specimens.

Microscopy

Whole-mount retinas were imaged using low magnification epifluorescence microscopy (E800; Nikon, Tokyo, Japan) before confocal imaging. Epifluorescence microscopy images were used for precise location of the retinal region, centered 3 mm superior to the optic disk (Fig. 1), before confocal microscopy studies. Such measures ensured that retinal eccentricity used for capillary morphometric comparisons was consistent in each eye donor.

Two Nikon C1 microscopes equipped with either three lasers (wavelengths 405, 488, and 532 nm) or four lasers (wavelengths 405, 488, 545, and 637 nm) were used for confocal imaging. Both microscopes were equipped with EZ-C1 software (v.3.20) (Nikon). Objective lenses that were used for confocal imaging included ×4 (NA 0.2), ×10 (NA 1.45), and ×20 (NA 0.75) Plan-Apo lenses (Nikon). Using

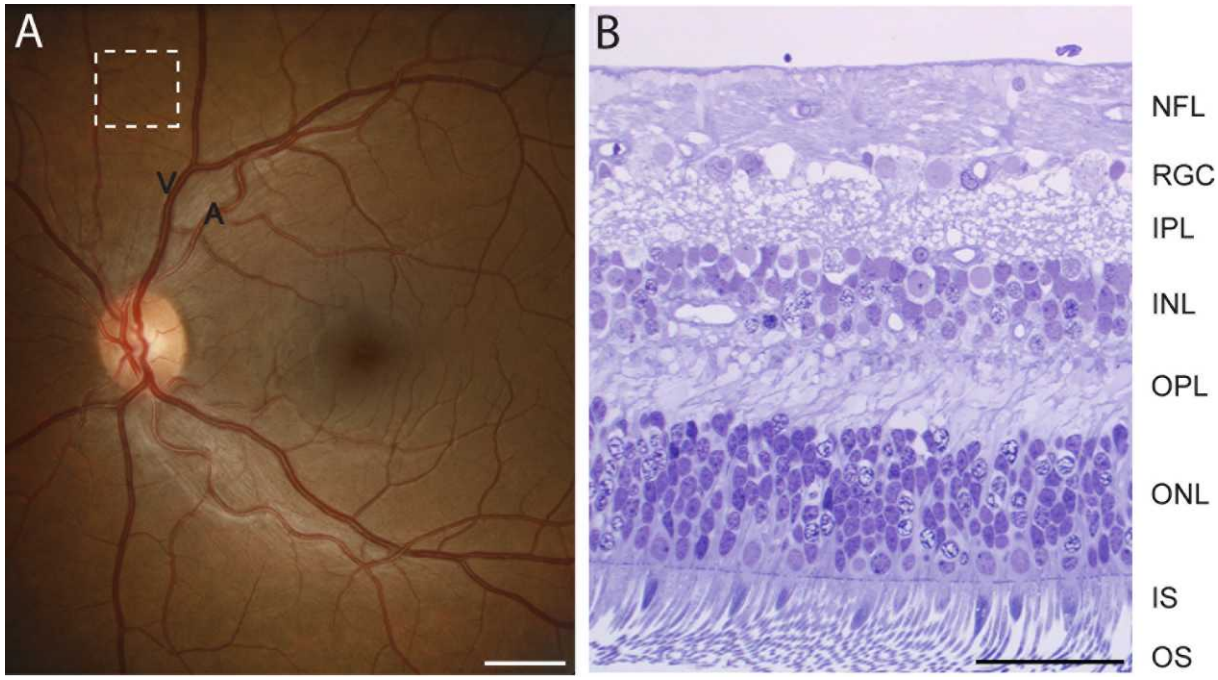

Figure 1. Region of study. Color fundus (**A**) and transverse retinal section (**B**) from healthy subjects demonstrate the clinical and histologic features, respectively, of the retinal eccentricity chosen for capillary morphometry analysis. A region 3 mm superior to the optic disk (*fenestrated box*) was examined. ONL, outer nuclear layer; IS, inner-segments of photoreceptors; OS, outer-segment of photoreceptors; A, artery; V, vein. *Scale bar*: 1000 μm (*color fundus*) and 50 μm (*histology*).

a motorized stage, a series of z-stacks were captured for each specimen beginning from the vitreal surface, at the level of the inner limiting membrane, to the outer retina. Each z-stack consisted of a depth of optical sections collected at 0.35 μm increments along the z-plane. Images of different wavelengths were acquired sequentially.

Image Preparation

ImagePro Plus (Version 7.1; Media Cybernetics, Rockville, MD) and Image J (version 1.43, available free online, National Institute of Health, in the public domain from http:/rsb.info.nih.gov/ij) were the image-analysis software that was used to quantify confocal microscope images. All images for the manuscript were prepared using Adobe Photoshop (version 12.1, Adobe Systems Inc., San Jose, CA) and Adobe Illustrator CS5 (version 12.1.0, Adobe Systems Inc.).

Study of Capillary Topography

Morphometric criteria used previously to define vascular plexuses in central nervous system and ocular studies were used to divide the retinal circulation into different capillary networks.[14–16,21] A change in capillary branching pattern[22,23] and projected orientation[14,23,24] was used to distinguish the different capillary networks. Additionally, using the movie-sequence function available on Image J software to view the z-stack sequentially, it was possible to determine if capillary networks displayed a laminar, single-planar orientation that was confined predominantly to a single retinal layer or if they displayed a complex three-dimensional configuration that traversed the z-axis. In this report, the term laminar refers to capillary configurations that are confined predominantly to a single plane with minimal projections along the z-axis. Likewise, the term three-dimensional refers to capillary networks that are not confined to a single plane, but instead demonstrate prominent projections along the vertical z-axis.

The movie-sequence function on Image J also was used to view capillary morphology simultaneously with nuclei and thereby locate the position of capillary networks within the retina. Transverse and flat-mount immunolabeling, with multiple antibodies, also was used to confirm the position of capillary networks relative to the nerve fiber layer (NFL), retinal ganglion cell (RGC) layer, bipolar cells, and horizontal cells.

Quantitative Study of Capillary Networks

A z-projected image of each capillary network together with previously defined histologic parameters,[7,13,16] was used to perform quantitative measurements. The following measurements were attained from each network as illustrated in Figure 2: Capillary diameter was defined as the perpendicular distance across the maximum chord axis of each vessel. Each image was partitioned into 9 equal areas and measurements were acquired from each area to ensure representative sampling. Capillary density was defined as percentage of the sample area occupied by vessel lumens.

Statistical Analysis

All data were expressed in terms of mean and SE, and were calculated using Sigmastat (Sigmastat, ver. 3.1; SPSS, Chicago, IL). Multiple measurements from eyes with data taken from right and left eyes of the same individual were analyzed using R (R Foundation for Statistical Computing, Vienna, Austria).[25] One-way ANOVA testing was performed to compare measurements between layers. The model used included "Right" or "Left" nested within "eye donor" as random effects using linear mixed modeling to test measurement differences between retinal layers.[25] The assignment of donor as a random effect was used to account for the effects of intra-"eye" correlation and similarly "Right" and "Left" to account for right and left eye correlation. Statistical analysis also determined if age accounted for differences in capillary diameter and vascular density measurements between retinal layers. We tested the influence of age upon density using a linear mixed model incorporating age as the predictive factor, and right and left eye as random factors to account for variation between right and left eye nested within donor eyes as another random factor. We also performed a one-way ANOVA testing the effect of cause of death upon vascular density using the same random effects model as

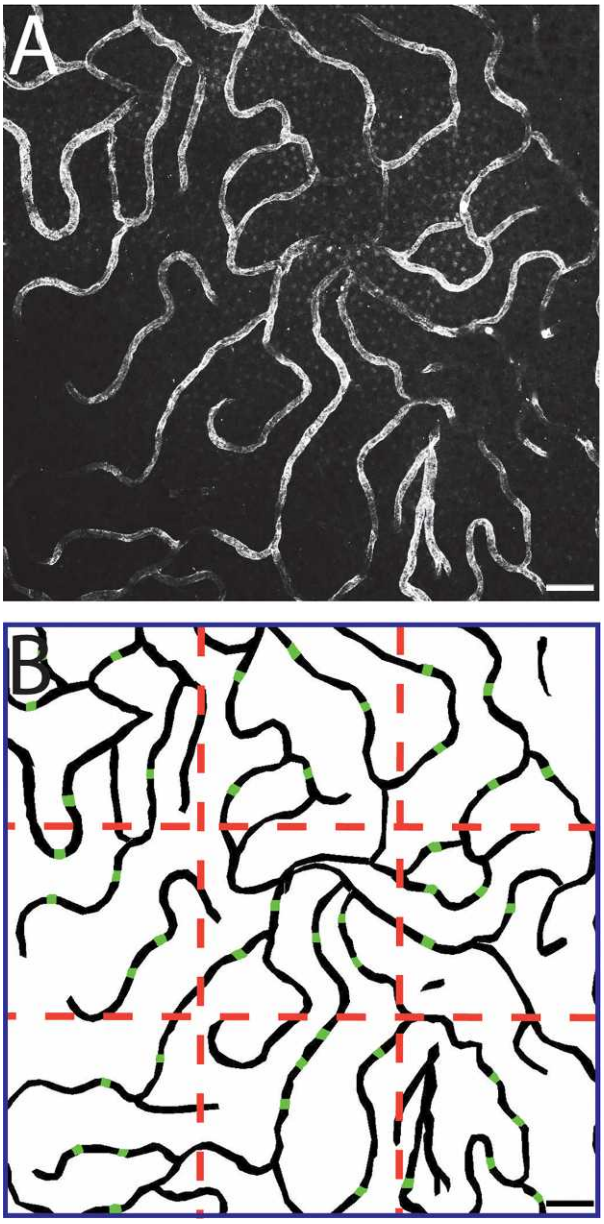

Figure 2. Quantification of capillary diameter and density. Confocal images of capillary networks (**A**) were traced manually (**B**) before quantitative analysis. Each traced image was divided into 9 equal areas (*red fenestrated lines*) to allow representative sampling of capillary diameter. The perpendicular distance across the maximum chord axis of each vessel was used to measure capillary diameter (*green*). The area occupied by capillary structures, as a proportion of the total image area, was used as a measure of capillary density and expressed as a percentage. *Scale bar*: 50 μm.

described above. Cause of death was defined as either accidental or cancer.

Results

General

The mean donor age was 49.71 ± 5.19 years. We examined 11 left and 5 right eyes from 12 male and 2 female donors. The mean postmortem time to initial perfusion ranged from 3 to 22 hours, with an average of 13.39 ± 1.68 hours.

All orders of the retinal microvasculature were well perfused after cannulation of the central retinal artery. Endothelial cells, smooth muscle cells, and nuclei of the retinal vasculature were labeled clearly.

Capillary Topography in the Human Retina

Morphometrically different capillary networks were identified consistently in the following locations: NFL, RGL, border of inner plexiform layer (IPL) and superficial boundary of the inner nuclear layer (INL), and boundary of deep INL and outer plexiform layer (OPL).

Capillaries in the NFL network were orientated parallel to the direction of RGC axon bundles and arose from branch vessels in the RGC layer. Capillaries in the NFL had linear trajectories with fewer intercapillary anastomotic connections compared to other networks (Fig. 3). Colocalization using γ-synuclein antibody confirmed that the location of this network was within the NFL. Within the retinal eccentricity examined in this study there was an observed reduction in capillary density in the NFL as the distance away from the optic disk increased (Fig. 3A).

In the RGC layer (Fig. 4), retinal arterioles clearly were observed to give rise to capillary networks. Retinal venules also were observed in this layer of the retina. Analysis of capillary trajectory in the RGC layer, using the movie-sequence function on Image J, demonstrated a complex vascular configuration. Many capillaries in the RGC layer projected along a single plane while some capillaries were observed to run obliquely at varying angles along the z-plane, and form anastomoses with capillary networks in the NFL and outer retina. The configuration of capillaries in the RGC network was significantly more three-dimensional than the NFL network. Capillary density also was observed to be greatest in the RGC capillary network.

The capillary network between the IPL and superficial portion of the INL also displayed a three-dimensional vascular configuration (Fig. 5). However, capillary density in this layer appeared significantly less than the RGC layer with a pronounced reduction in the number of vessels that projected along a single plane. Colocalization studies using ON-bipolar cell marker demonstrated that capillaries in this layer were situated among bipolar cell processes.

The deepest capillary network was found at the level of horizontal cells in the INL (Fig. 6). Colocalization studies using Go-α antibody revealed that synapses of ON-bipolar cells were distributed among the capillary network. Similar to the NFL network, capillaries in this layer demonstrated predominantly a laminar configuration with most capillaries projecting along a single plane. Multiple closed loops also were observed in this capillary network.

Quantitative Analysis of Capillary Diameter

Mean capillary diameter for all networks was 8.26 ± 0.03 μm. Table 2 provides mean capillary diameter for each capillary network. Capillary diameter in the NFL network was significantly greater than in the RGC ($P < 0.001$) and IPL ($P < 0.001$) networks. Capillary diameter in the deep INL network also was significantly greater than in the RGC ($P < 0.001$) and IPL ($P < 0.001$) networks. There was no difference in capillary diameter between the NFL and deep INL networks ($P = 0.227$), and RGC and IPL networks ($P = 0.740$). Age did not influence capillary diameter in any of the networks (all $P > 0.050$).

Table 3 provides mean capillary diameter for patients deceased from cancer or accidental means. There was no difference in capillary diameter between the two groups in the RGC ($P = 0.303$), NFL ($P = 0.874$), IPL ($P = 0.964$), and deep INL ($P = 0.183$) networks.

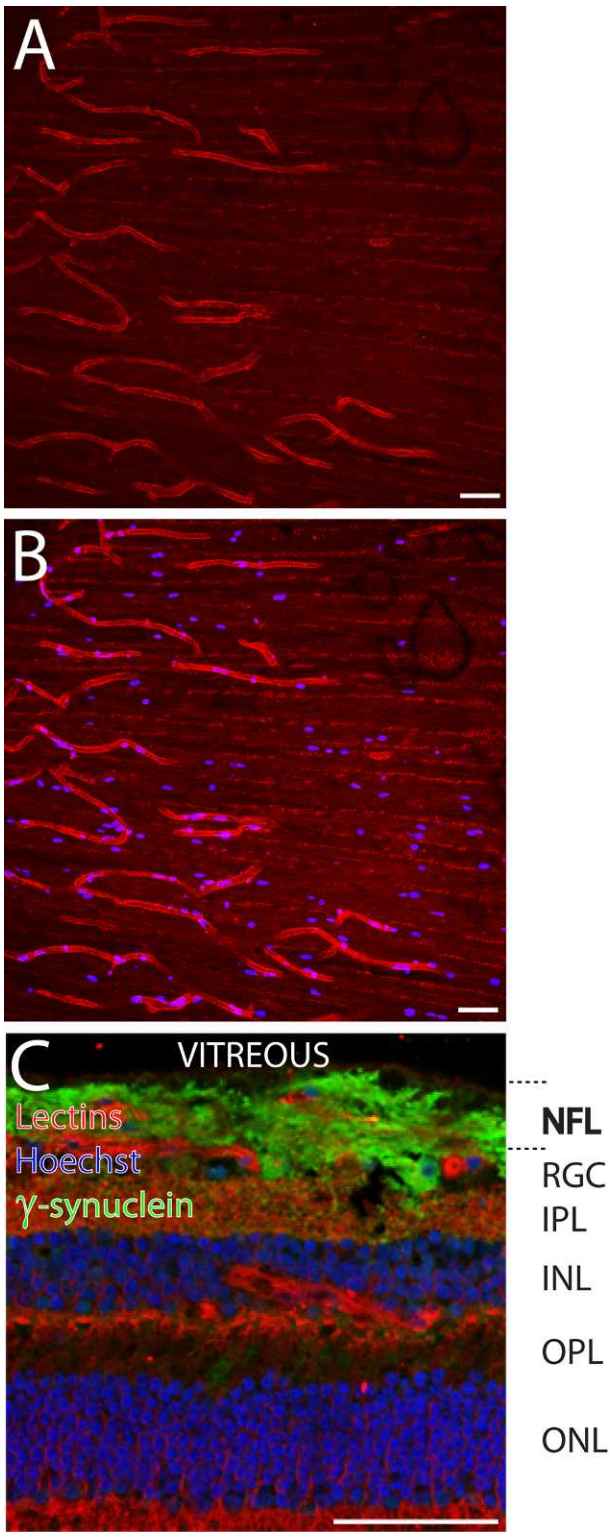

Figure 3. NFL capillary network. (**A**) Whole-mount confocal microscope image captured from a single laser channel demonstrates the linear trajectory of capillaries and the relative absence of anastomotic connections between vessels. There is a reduction in the density of capillaries as the distance away from optic disk increases (*left-to-right direction in image*). (**B**) Merged image with nuclei information demonstrates a paucity of cells in this region. (**C**) Triple-stained transverse retinal section demonstrates the location of this network within the NFL. Lectins stain endothelium, Hoechst stain nuclei, and γ-synuclein stain RGC axons. *Scale bar*: 50 μm.

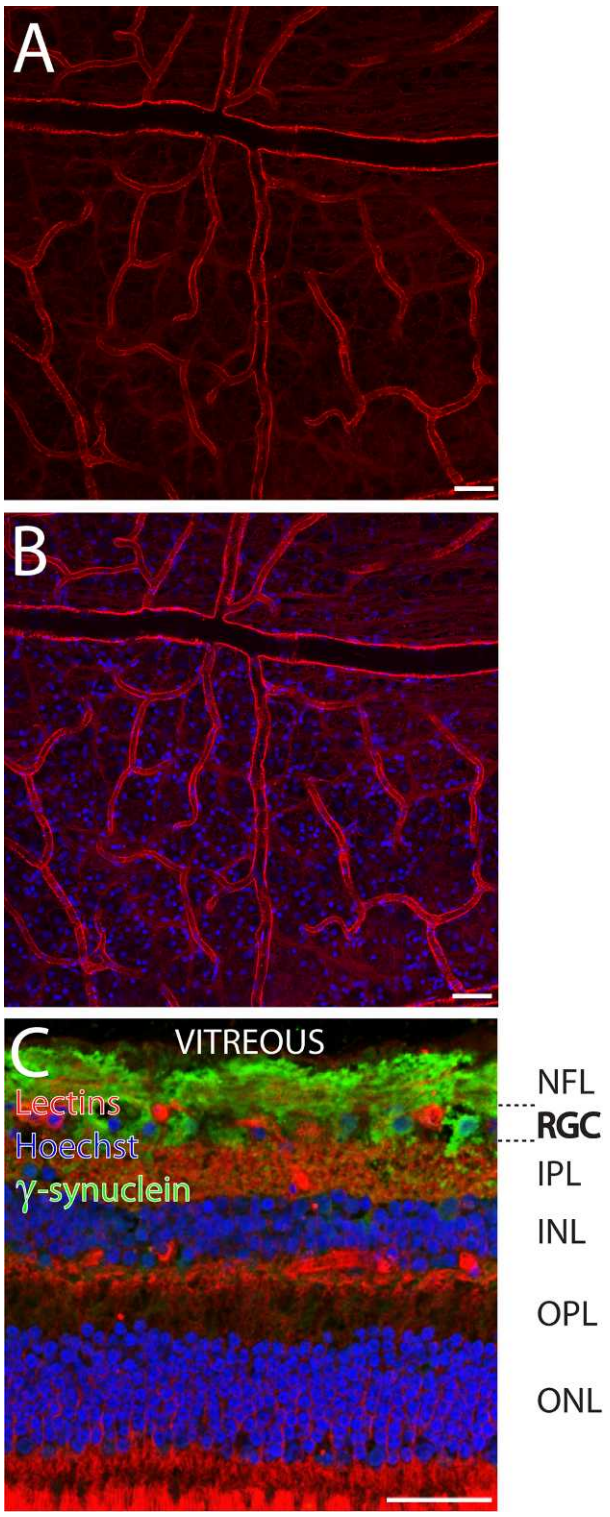

Figure 4. RGC layer capillary network. (**A**) Whole-mount confocal microscope image captured from a single laser channel demonstrates the high density of capillaries in this network. Arterioles and venules also are observed in addition to capillaries. (**B**) Merged image with nuclei information demonstrates a high density of cells in this region. (**C**) Triple-stained transverse retinal section demonstrates the location of this network within the RGC layer. Lectins stain endothelium, Hoechst stain nuclei, and γ-synuclein stain RGCs. *Scale bar*: 50 μm.

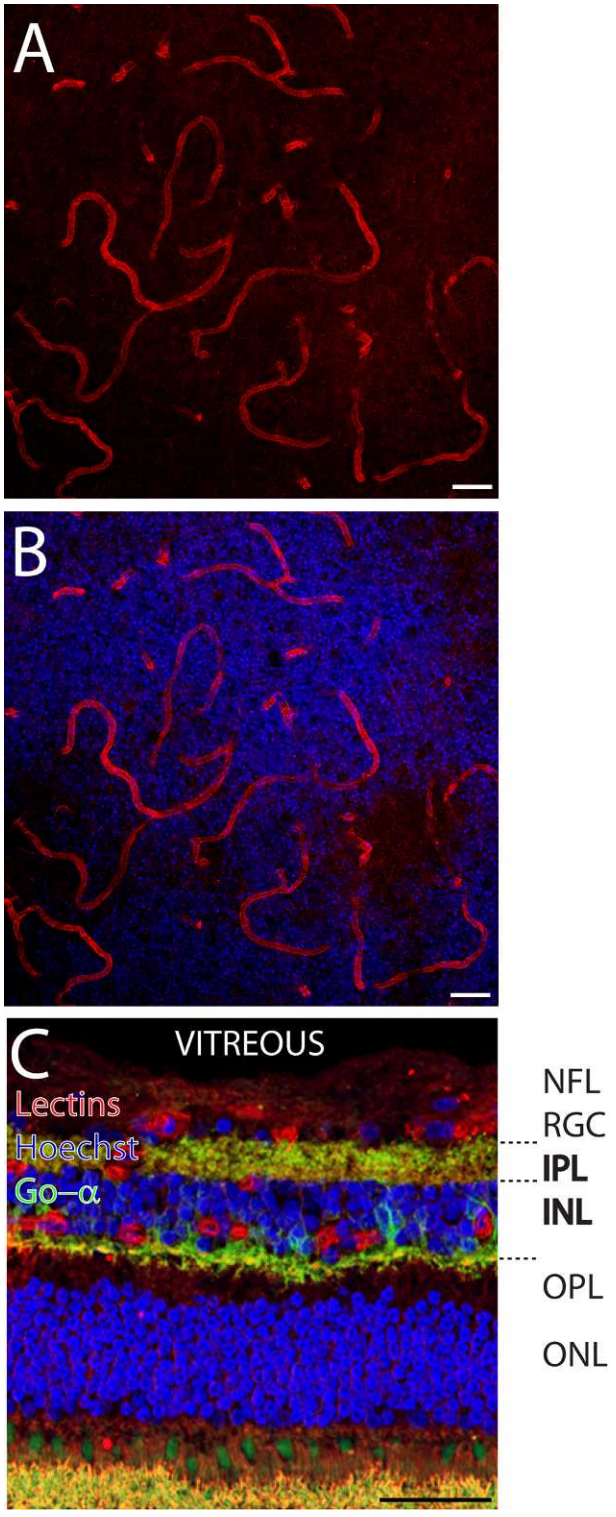

Figure 5. IPL and superficial INL capillary network. (**A**) Whole-mount confocal microscope image captured from a single laser channel demonstrates the low density of capillaries in this network. (**B**) Merged image with nuclei information demonstrates a large number of cells in this region. (**C**) Triple-stained transverse retinal section demonstrates that this network is located at the boundary between the IPL and INL. Lectins stain endothelium, Hoechst stain nuclei, and Go-α stain ON-bipolar cells. *Scale bar*: 50 μm.

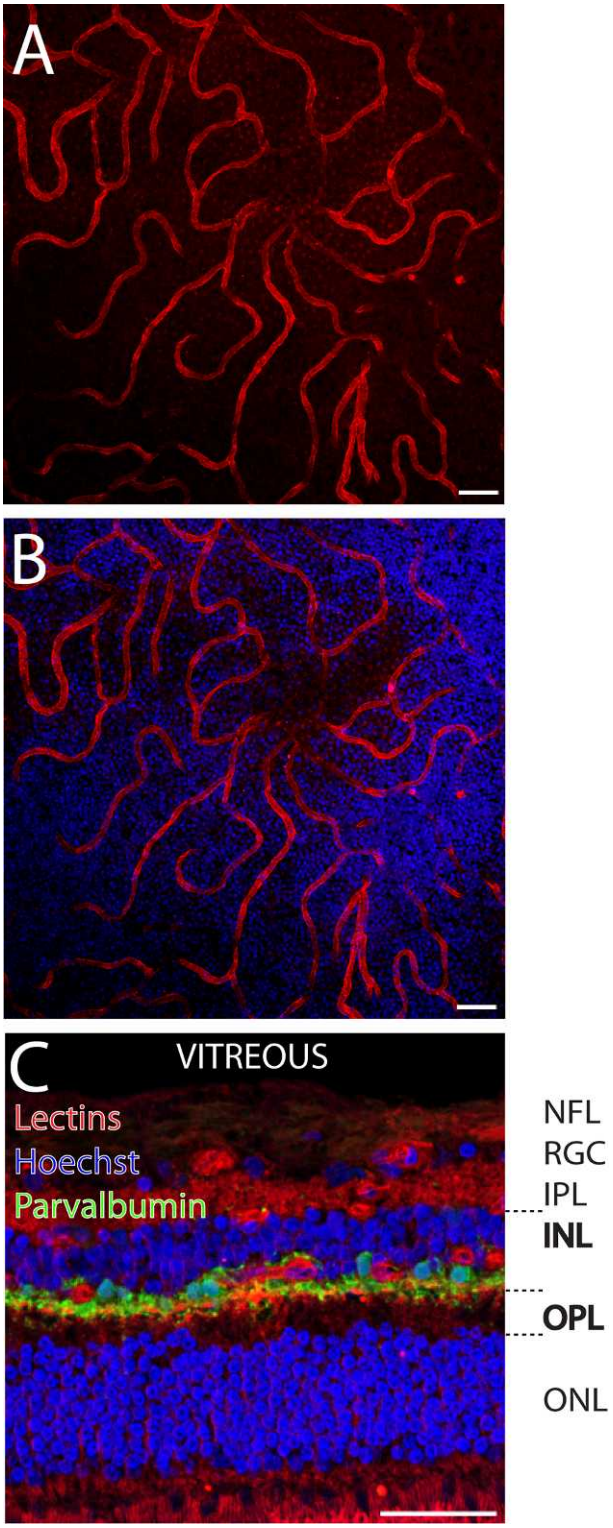

Figure 6. Deep INL and OPL capillary network. (**A**) Whole-mount confocal microscope image captured from a single laser channel demonstrates the planar configuration of this network with multiple closed capillary loops. (**B**) Merged image with nuclei information demonstrates a high density of cells in this region. (**C**) Triple-stained transverse retinal section demonstrates that this network is located at the boundary between the INL and OPL. Lectins stain endothelium, Hoechst stain nuclei, and Parvalbumin stain horizontal cells. *Scale bar*: 50 μm.

Table 2. Quantitative Capillary Diameter and Density Data for Each Network

Capillary Network	NFL	RGC	IPL / Superficial INL	Deep INL/OPL
Capillary diameter (μm)	8.47 ± 0.05 (540)	8.01 ± 0.05 (540)	7.99 ± 0.06 (540)	8.56 ± 0.06 (540)
Capillary density (%)	13.69 ± 0.01 (12)	26.74 ± 0.01 (12)	11.28 ± 0.01 (12)	16.12 ± 0.01 (12)

Mean and SE for NFL, RGC layer, IPL and superficial INL (IPL/superficial INL), and deep INL and outer OPL (deep INL/OPL) networks is provided. Numbers in parentheses indicate sample number for each measurement.

Quantitative Analysis of Capillary Density

Table 2 provides mean density measurements for each capillary network. Capillary densities were significantly different between networks. Capillary density was greatest in the RGC network, and was significantly greater than the NFL ($P < 0.001$), IPL ($P < 0.001$), and deep INL ($P < 0.001$) networks. Capillary density was lowest in the IPL network and was significantly lower than the deep INL network ($P < 0.001$). NFL capillary density also was greater than the IPL network ($P = 0.036$). Age did not influence capillary density in any of the networks (all $P > 0.050$).

Table 3 provides mean capillary density for patients deceased from cancer and accidental means. There was no difference in capillary density between the two groups in the RGC ($P = 0.660$), NFL ($P = 0.886$), and IPL ($P = 0.455$) networks. Capillary density was significantly greater in the cancer group in the deep INL network ($P = 0.046$).

Discussion

Capillary networks in the human retina are required to support the immense energy demands of neuronal components without compromising the optical integrity of the light pathway to the outer retina. In this regard, the function served by the retinal circulation is significantly different from other capillary networks in the central nervous system (CNS). Oxygen tension and demands within the retina markedly are heterogeneous,[9] and the metabolic demands of distinct retinal layers are satisfied most likely, to varying extents, by capillary adaptations that function to increase the efficiency of regional nutrient delivery and waste removal. Therefore, studying morphometric variations between capillary networks may provide vital information concerning the energy requirements of regional neuronal structures via effective neurovascular coupling mechanisms. It also may allow useful structure-function extrapolations between capillary morphometry and previously determined measurements on retinal metabolism[3–8,26–29] to be performed.

Previous investigators have used a variety of different techniques to document the organization of capillary networks in the primate retina. Trypsin digest[30] and corrosion casting[31] techniques have provided valuable information concerning the three-dimensional morphology of capillary networks, however, inadvertent tissue damage as a result of these techniques limited localization of capillary networks respective to retinal layers. Fluorescein angiography[32] and magnetic resonance imaging[33] have been used recently to study the retinal circulation; however, the limited resolution offered by these techniques again precluded study at a cellular level and restricted colocalization. A major advantage of the methodology used in our study is that it allows complete labeling of the retinal microcirculation without inadvertently altering surrounding nonvascular structures. Triple-labeling of post-perfused tissue also allowed accurate identification of capillary network location within the retina and confirmed what was demonstrated on flat-mount confocal microscope images.

There have been varying reports concerning the order and number of capillary networks in the human retina. Early trypsin digest studies by Toussaint et al. demonstrated a lack of capillary lamination,[34] while Michaelson et al. demonstrated a two-layered laminar pattern using benzidine peroxidase techniques.[35] The histologic details reported in these studies most likely were limited to some extent by the microscopic and immunohistochemical techniques that were available at the time. Snodderly et al.[15,16] and Gariano et al.[10] published excellent studies in the 1990s, and demonstrated two inner and two outer capillary beds in human and nonhuman primate retinae. Our findings reaffirm that of the latter 2 groups, and demonstrate four morphometrically different capillary networks in the human retina being present in the following regions: NFL, RGC layer, border of IPL and superficial boundary of INL, and boundary of deep INL and OPL. Similar to these previous investigators,[10,15,16] we found that the innermost and outermost capillary networks displayed a single, planar configuration, while that of the RGC and IPL demonstrated a complex three-dimensional configuration. Three-dimensional vascular configurations are believed to increase the efficiency of oxygen transfer and waste removal in metabolically active tissues.[21,23] The variation in retinal capillary network morphology identified in our study demonstrated important parallels to the human cerebral cortex where the microcirculation is adapted in accordance with regional neuronal demands.[24,36,37] Previous researchers have shown that the inner 1 mm of cerebral cortex demonstrates large meshes, the next 2 mm are filled with fine polygonal meshes, and the outer 0.1 mm contains large quadrangular meshes that run parallel to the surface.[24,36,37] Taken together our findings suggested that, similar to the brain, capillary networks in the retina are morphometrically adapted to serve the unique functional demands of each retinal layer.

Using confocal microscope techniques and image analysis software, we were able to quantify the morphometric characteristics of each capillary network and, thus, extend

Table 3. Morphometric Comparisons between Cancer-Death and Accidental-Death Groups

Capillary Network	NFL		RGC		IPL / Superficial INL		Deep INL/OPL	
Cause of death	Accidental	Cancer	Accidental	Cancer	Accidental	Cancer	Accidental	Cancer
Capillary diameter (μm)	8.30 ± 0.08	8.64 ± 0.08	8.02 ± 0.07	8.01 ± 0.07	7.98 ± 0.08	8.00 ± 0.08	8.34 ± 0.08	8.78 ± 0.08
Total capillary density (%)	13.17 ± 0.01	14.22 ± 0.01	27.25 ± 0.02	26.23 ± 0.02	10.81 ± 0.01	11.75 ± 0.01	14.72 ± 0.01	17.52 ± 0.00

Mean and SE for NFL, RGC layer, IPL and superficial INL (IPL/superficial INL), and deep INL and OPL (deep INL/OPL) networks is provided. Capillary density in the deep INL/OPL network was significantly different between the two groups.

on the observations made by previous investigators. We identified significant differences in capillary diameter among all four networks, with the smallest capillary diameter being present in the RGC and IPL networks. Mean capillary diameter is one measure of the rate at which a capillary network is able to exchange oxygen per unit volume of blood.[38] A reduction in capillary diameter increases the surface area-to-blood volume ratio, resulting in greater oxygen exchange area for a given amount of blood. In the brain, differences in intracortical capillary network diameters correlate with regional variations in neuronal function.[39] Lower mean diameters of capillary networks in RGC and IPL layers suggested high rates of oxygen exchange in this region of the retina. These morphometric findings correlated with our previous in vivo functional studies, in which we demonstrated high oxygen uptake in the IPL.[9] Capillary diameter measurements in our study also were greater than in previous reports[15,16] and may reflect inter-species and tissue preparation differences.

Within the grey matter of the CNS an increase in capillary density correlates strongly with an increase in blood flow and mitochondrial activity.[40] Histologic studies have shown significant variation in vascular density across neuronal layers in the brain.[41] Total capillary density in the nonhuman primate fovea, peri-fovea and peripapillary region has been measured as 40%, 45%, and 60 to 70% of cases, respectively.[15,16] Vascular density also is known to vary depending on the eccentricity from central retina.[10] To our knowledge, there have not been previous capillary density measurements of individual networks in the human retina. In our study, capillary density was greatest in the RGC layer implicating it as a metabolically intense region. The dependency of RGCs on a high density capillary circulation may be one reason why this subset of neurons could be vulnerable particularly to acute, transient and mild hypoxic stress.[42]

Although our study provided important new knowledge regarding retinal capillary topography in human eyes, we acknowledge several limitations of the report. Firstly, the sample size of our study is relatively small and consists of only 16 human eyes. It is difficult to acquire human eyes from healthy individuals and we did not wish to waste human tissue by performing an extensive analysis when appropriate statistical tests permitted us to identify reliably differences between capillary networks, despite the relative small sample size. The other limitation of our work is that only one retinal eccentricity was examined. The aim of our study was to quantify the morphometric characteristics of capillary networks, and speculate upon structure-function relationships between vascular units and regional metabolic activity. It is expected that the morphometric characteristics of capillary networks will vary according to retinal eccentricity especially in specialized regions of the retina, such as the fovea, macula, and immediate peripapillary tissue. Similar to the report by Snodderly et al.,[15,16] we observed a change in the NFL capillary network in a proximal-distal direction. Gariano et al. demonstrated that deeper vascular layers disappear in the peripheral retina.[10] Therefore, examination of the far peripheral retina possibly may demonstrate significant alterations to capillary networks.

Our study provided important insights into vascular mechanisms relevant to retinal homeostasis. We demonstrated that mode of death was a significant factor in determining capillary density, and it is expected that regional capillary networks will be altered by ocular and systemic disease. Therefore, it will be important to perform similar studies using diseased human eyes as it may enhance our understanding of capillary-mediated mechanisms in retinal vascular disease.

Acknowledgements

The staff of the Lions Eye Bank of Western Australia, Lions Eye Institute provided human donor eyes. The staff of DonateWest, the Western Australian agency for organ and tissue donation, facilitated the recruitment of donors into the study by referral and completion of consent processes. Dean Darcey provided expert technical assistance.

References

1. Attwell D, Buchan AM, Charpak S, Lauritzen M, Macvicar BA, Newman EA. Glial and neuronal control of brain blood flow. *Nature*. 2010;468:232–243.
2. Gordon GR, Choi HB, Rungta RL, Ellis-Davies GC, Macvicar BA. Brain metabolism dictates the polarity of astrocyte control over arterioles. *Nature*. 2008;456:745–749.
3. Yu DY, Cringle SJ, Alder VA, Su EN. Intraretinal oxygen distribution in rats as a function of systemic blood pressure. *Am J Physiol*. 1994;36:H2498–H2507.
4. Yu DY, Cringle SJ. Oxygen distribution in the mouse retina. *Invest Ophthalmol Vis Sci*. 2006;47:1109–1112.
5. Yu DY, Cringle SJ, Su EN. Intraretinal oxygen distribution in the monkey retina and the response to systemic hyperoxia. *Invest Ophthalmol Vis Sci*. 2005;46:4728–4733.
6. Cringle SJ, Yu PK, Su EN, Yu DY. Oxygen distribution and consumption in the developing rat retina. *Invest Ophthalmol Vis Sci*. 2006;47:4072–4076.
7. Yu DY, Cringle SJ. Retinal degeneration and local oxygen metabolism. *Exp Eye Res*. 2005;80:745–751.
8. Yu DY, Cringle SJ, Yu PK, Su EN. Intraretinal oxygen distribution and consumption during retinal artery occlusion and graded hyperoxic ventilation in the rat. *Invest Ophthalmol Vis Sci*. 2007;48:2290–2296.
9. Yu DY, Cringle SJ. Oxygen distribution and consumption within the retina in vascularised and avascular retinas and in animal models of retinal disease. *Prog Retina Eye Res*. 2001; 20:175–208.
10. Gariano RF, Iruela-Arispe ML, Hendrickson AE. Vascular development in primate retina: comparison of laminar plexus formation in monkey and human. *Invest Ophthalmol Vis Sci*. 1994;35:3442–3455.
11. Yu PK, Balaratnasingam C, Cringle SJ, McAllister IL, Provis J, Yu DY. Microstructure and network organization of the microvasculature in the human macula. *Invest Ophthalmol Vis Sci*. 2010;51:6735–6743.
12. Yu PK, Balaratnasingam C, Morgan WH, Cringle SJ, McAllister IL, Yu DY. The structural relationship between the microvasculature, neurons, and glia in the human retina. *Invest Ophthalmol Vis Sci*. 2010;51:447–458.
13. Yu PK, Tan PE, Morgan WH, Cringle SJ, McAlliser IL, Yu DY. Age-related changes in venous endothelial phenotype at human retinal artery-vein crossing points. *Invest Ophthalmol Vis Sci*. 2012;53:1108–1116.
14. Hogan MJ, Alvarado JA, Esperson Weddell J. *Histology of the Human Eye: An Atlas and Textbook*. Philadelphia, W.B. Saunders Company;1971.
15. Snodderly DM, Weinhaus RS. Retinal vasculature of the fovea of the squirrel monkey, Saimiri sciureus: three-dimensional architecture, visual screening, and relationships to the neuronal layers. *J Comp Neurol*. 1990;297:145–163.
16. Snodderly DM, Weinhaus RS, Choi JC. Neural-vascular relationships in central retina of macaque monkeys (Macaca fascicularis). *J Neurosci*. 1992;12:1169–1193.
17. Gariano RF, Iruela-Arispe ML, Sage EH, Hendrickson AE. Immunohistochemical characterization of developing and mature primate retinal blood vessels. *Invest Ophthalmol Vis Sci*. 1996;37:93–103.

18. Xiao M, Hendrickson A. Spatial and temporal expression of short, long/medium, or both opsins in human fetal cones. *J Comp Neurol*. 2000;425:545–559.
19. Surgucheva I, Weisman AD, Goldberg JL, Shnyra A, Surguchov A. Gamma-synuclein as a marker of retinal ganglion cells. *Mol Vis*. 2008;14:1540–1548.
20. Haverkamp S, Haeseleer F, Hendrickson A. A comparison of immunocytochemical markers to identify bipolar cell types in human and monkey retina. *Vis Neurosci*. 2003;20:589–600.
21. Rackl A, Pawlik G, Bing RJ. Cerebral capillary topography and red cell flow in vivo. In: Ceros-Navaroo J, Fritschka E, eds. *Cerebral Microcirculation and Metabolism*. New York, NY: Raven Press; 1981:17–21.
22. Richard E, van Gool WA, Hoozemans JJ, et al. Morphometric changes in the cortical microvascular network in Alzheimer's disease. *J Alzheimers Dis*. 2010;22:811–818.
23. Shaver SW, Pang JJ, Wall KM, Sposito NM, Gross PM. Subregional topography of capillaries in the dorsal vagal complex of rats: I. Morphometric properties. *J Comp Neurol*. 1991;306:73–82.
24. Cerebral Circulation. A critical discussion of the symposium. In: Cobb S, ed. *The Circulation of the Brain and Spinal Cord*. Baltimore, MD: Williams and Wilkins; 1938:710–752.
25. R Development Core Team. *R: A Language and Environment for Statistical Computing*. Vienna, Austria: R Foundation for Statistical Computing; 2011.
26. Yu DY, Cringle SJ, Alder VA, Su EN, Yu PK. Intraretinal oxygen distribution and choroidal regulation in the avascular retina of guinea pigs. *Am J Physiol*. 1996;270:H965–H973.
27. Yu DY, Cringle SJ. Low oxygen consumption in the inner retina of the visual streak of the rabbit. *Am J Physiol (Heart C)*. 2004;286:H419–H423.
28. Yu DY, Cringle SJ, Su EN, Yu PK, Humayun MS, Dorin G. Laser-induced changes in intraretinal oxygen distribution in pigmented rabbits. *Invest Ophthalmol Vis Sci*. 2005;46:988–999.
29. Yu DY, Cringle SJ, Su EN, Yu PK. Retinal oxygen distribution in a rat model of retinal ischemia. *Invest Ophthalmol Vis Sci*. 2000;41:S19.
30. Danis RP, Wallow IHL. HRP/trypsin technique for studies of the retinal vasculature. *Invest Ophthalmol Vis Sci*. 1986;27:434–437.
31. Bek T, Jensen PK. Three-dimensional structure of human retinal vessels studied by vascular casting. *Acta Ophthalmol (Copenh)*. 1993;71:506–513.
32. Mendis KR, Balaratnasingam C, Yu P, et al. Correlation of histologic and clinical images to determine the diagnostic value of fluorescein angiography for studying retinal capillary detail. *Invest Ophthalmol Vis Sci*. 2010;51:5864–5869.
33. Cheng H, Nair G, Walker TA, et al. Structural and functional MRI reveals multiple retinal layers. *Proc Natl Acad Sci U S A*. 2006;103:17525–17530.
34. Toussaint D, Kuwabara T, Cogan DG. Retinal vascular patterns. II Human retinal vessels studied in three dimensions. *Arch Ophthalmol*. 1961;65:137–143.
35. Michaelson IC, Campbell ACP. The anatomy of the finer retinal vessels, and some observations on their significance in certain retinal diseases. *Trans Ophthalmol Soc UK*. 1940;60:71–112.
36. Craigie EH. The vascularity of the cerebral cortex of the albino rat. *J Comp Neurol*. 1921;33:193–212.
37. Motti ED, Imhof HG, Yaşargil MG. The terminal vascular bed in the superficial cortex of the rat. An SEM study of corrosion casts. *J Neurosurg*. 1986;65:834–846.
38. Bell MA, Ball MJ. Morphometric comparison of hippocampal microvasculature in ageing and demented people: diameters and densities. *Acta Neuropathol*. 1981;53:299–318.
39. Pawlik G, Rackl A, Bing RJ. Quantitative capillary topography and blood flow in the cerebral cortex of cats: an in vivo microscopic study. *Brain Res*. 1981;208:35–58.
40. Tuor UI, Kurpita G, Simone C. Correlation of local changes in cerebral blood flow, capillary density, and cytochrome oxidase during development. *J Comp Neurol*. 1994;342:439–448.
41. Weber B, Keller AL, Reichold J, Logothetis NK. The microvascular system of the striate and extrastriate visual cortex of the macaque. *Cereb Cortex*. 2008;18:2318–2330.
42. Kergoat H, Herard ME, Lemay M. RGC sensitivity to mild systemic hypoxia. *Invest Ophthalmol Vis Sci*. 2006;47:5423–5427.